Journal of Inorganic and Organometallic Polymers and Materials (2021) 31:303–310
https://doi.org/10.1007/s10904-020-01702-7

Facile Synthesis of SnO_2/SiC Nanosheets for Photocatalytic Degradation of MO

Taichao Zhang[1] · Zhen Dai[1] · Baoyan Liang[1] · Yunchao Mu[1]

Received: 28 May 2020 / Revised: 19 July 2020 / Accepted: 4 August 2020 / Published online: 12 August 2020

Abstract
Novel SnO_2/SiC photocatalysts with nanosheet morphology were successfully fabricated by mechanical alloying and subsequent aging of $SnCl_2{\cdot}2H_2O$, NH_4HCO_3, SiC, and 2-methylimidazole powders. The photocatalysts were mainly composed of SiC and SnO_2. When the SiC content of the raw materials was higher, small amounts of $Sn_6O_4(OH)_4$ also existed in the product. TEM results show that SiC nanocrystallines were well combined with SnO_2 nanosheets. These SnO_2/SiC photocatalysts showed good photocatalytic degradation efficiency to methyl orange (MO) under visible-light irradiation. The MO was rapidly reduced by 99% within 45 min by SiC/SnO_2 composite. The excellent photocatalytic performance was mainly attributed to the formation of SnO_2/SiC heterojunction, which reduced the recombination of photogenerated electrons and holes.

Keywords SiC · SnO_2 · Photocatalytic

1 Introduction

Dye wastewater pollution has attracted increasing attention due to the rapid development of printing and dyeing industry. At present, the main methods for treatment of dye wastewater are adsorption, chemical oxidation, ultrasonic degradation, biological degradation, and photocatalytic oxidation. Photocatalytic oxidation [1] has the unique advantages of low energy consumption and high degradation efficiency; this method has gained increasing attention in the academia and production enterprises. Research and development of semiconductor catalysts, such as TiO_2 [2–5], is the core of photocatalytic oxidation for dye wastewater treatment. SnO_2 is a wide band gap semiconductor (Eg = 3.6 eV) and has excellent photoelectric performance and chemical stability; as such, SnO_2 is a common photocatalytic material [6, 7]. However, some disadvantages of SnO_2 that seriously limit its application in the field of photocatalysis include fast recombination of carrier and hole pairs, low light conversion efficiency, and low visible-light response. Different semiconductors with band structure have been matched to build heterostructures with improved photocatalytic efficiency [8, 9]. At present, SnO_2 is combined with TiO_2 [10], ZnO [11], Fe_2O_3 [12], C_3N_4 [13], graphene [14], and other materials to obtain significantly improved visible photocatalytic performance.

SiC, as a traditional non-metallic semiconductor material, is rich in carbon and silicon and found in the Earth's crust. SiC has high carrier transport rate and chemical stability and is thus a potential photocatalyst [15, 16]. SiC and SnO_2 have matching conduction band and valence band potentials. SiC/SnO_2 composites can be used in photocatalytic water splitting [17, 18] and electrochemical oxidation of wastewater [19]. However, no report is available about heterojunction materials constructed by SnO_2 and SiC for photocatalytic degradation.

In our previous study [20], $Sn_6O_4(OH)_4$ powders were prepared by mechanical alloying with $SnCl_2{\cdot}2H_2O$ and NH_4HCO_3 as raw materials; SnO_2 nanoparticles were obtained by aging $Sn_6O_4(OH)_4$ powders at a certain time in air. However, the as-synthesized SnO_2 material did not have visible-light catalytic degradation performance. In the present study, we prepared SnO_2/SiC composites through mechanical alloying and subsequent aging. The visible-light photocatalytic degradation of methyl orange (MO) was also studied.

✉ Baoyan Liang
6210@zut.edu.cn

[1] Materials and Chemical Engineering School, Zhongyuan University of Technology, Zhengzhou 450007, People's Republic of China

2 Experimental Procedure

Reagent-grade $SnCl_2{\cdot}2H_2O$, 2-methylimidazole, and NH_4HCO_3 were obtained from Tianjin Beichen Fangzheng Reagent Factory. SiC powders (average size of 40 nm, 99.9% purity) were purchased from Beijing Deke Island Gold Technology Co., Ltd. The raw material formula is listed in Table 1. These raw material powders were weighted and mechanically ground on a small grinder for 25 min. The ground powders were allowed to stand in air for 30 min before immersing in deionized water for 10 days. Finally, the powders were washed several times and dried. The obtained powders were named SnO_2, 1% SiC/SnO_2, 3% SiC/SnO_2, 5% SiC/SnO_2, 7% SiC/SnO_2, 9% SiC/SnO_2, and 11% SiC/SnO_2. The detailed test equipment and conditions were reported in previous research [16]. In the present work, the concentrations of the photocatalyst and MO are 1 g/L and 15 mg/L, respectively.

Table 1 Raw material formula

Sample name	$SnCl_2 \cdot 2H_2O$	NH_4HCO_3	2-Methyl-imidazole	SiC
SnO_2	2.25	1.6	1.23	0
1% SiC/SnO_2	2.25	1.6	1.23	0.014
3% SiC/SnO_2	2.25	1.6	1.23	0.043
5% SiC/SnO_2	2.25	1.6	1.23	0.074
7% SiC/SnO_2	2.25	1.6	1.23	0.105
9% SiC/SnO_2	2.25	1.6	1.23	0.138
11% SiC/SnO_2	2.25	1.6	1.23	0.173

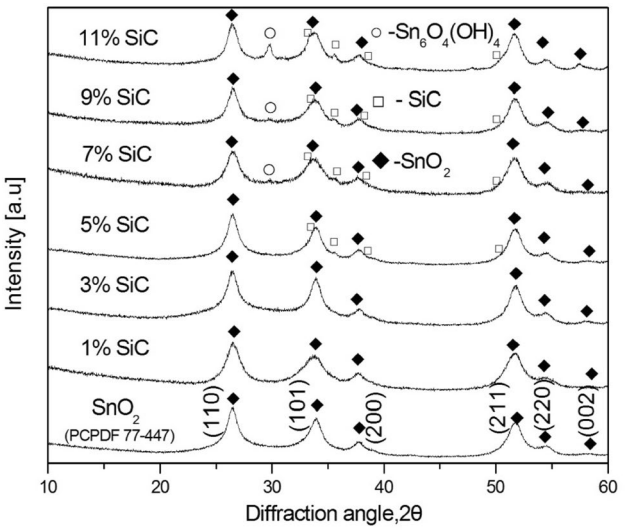

Fig. 1 The XRD patterns of SiC/SnO_2 composites

3 Results and Discussion

Figure 1 shows that the XRD pattern of different photocatalytic materials. The synthesized products were mainly composed of SnO_2 and SiC. MA-synthesized $Sn_6O_4(OH)_4$ precursor was basically transformed to SnO_2 by aging. The reaction equation for the formation of SnO_2 was as follows.

$$6SnCl_2 \cdot 2H_2O + 12NH_4HCO_3 \rightarrow Sn_6O_4(OH)_{t4} + 12NH_4Cl + 16H_2O + 12CO_2 \quad (1)$$

$$Sn_6O_4(OH)_4 + 3O_2 \rightarrow 6SnO_2 + 2H_2O \quad (2)$$

Compared with other fabrication technologies [10–14], this aging technology had the advantages of mild conditions, cost-effectiveness, and simplicity.

When the SiC content was low (≦2%), the SiC peaks were difficult to find. The SiC peaks began to appear when the SiC content was 4%. With increasing SiC content, the intensity of the diffraction peaks of SiC increased. Weak $Sn_6O_4(OH)_4$ peak began to appear when the SiC content was increased to 7%. The intensity of the $Sn_6O_4(OH)_4$ peak obviously increased when the SiC content was increased to 11%. Hence, adding excess SiC may inhibit the transformation from $Sn_6O_4(OH)_4$ into SnO_2 and could degrade the photocatalytic properties of the composites.

The diffraction peaks of SnO_2 widened, indicating the fine grains of SnO_2. Average grain size was estimated from the highest intensity peaks of SnO_2 ($2\theta = 26.56°$) by using the Scherrer's equation. The average grain sizes were 6–7 nm for SnO_2 and SnO_2/SiC composites. Hence, we obtained very fine SnO_2 nanocrystallines by using the proposed method.

Figure 2 shows the SEM images of (a) SnO_2 and (b) 7%SnO_2/SiC composite and present similar serious aggregates. These aggregates were composed of nanoparticles with size of several to dozens of nanometer.

Figure 3a shows that the as-synthesized SnO_2 mainly consisted of severely agglomerated nanocrystallines with size of less than 10 nm; this finding is consistent with the XRD results. Nanosheets with thickness of about 3 nm and length of about 30 nm were also detected. The TEM image (Fig. 3b) of 7%SnO_2/SiC composite was identical to that of the SnO_2 sample. Figure 3c shows the HRTEM image of 7%SnO_2/SiC composite. The tight interface of SiC and SnO_2 was observed, indicating the formation of a good heterostructure. This SnO_2/SiC heterostructure may enhance the separation of photoelectron pairs, thereby enhancing the photocatalytic performance.

The compositional information and elemental chemical states of 7% SiC/SnO_2 were probed with X-ray photoelectron spectroscopy (XPS). Spectrum decomposition was performed using the casaXPS program with Gaussian functions after the subtraction of a Shirley background.

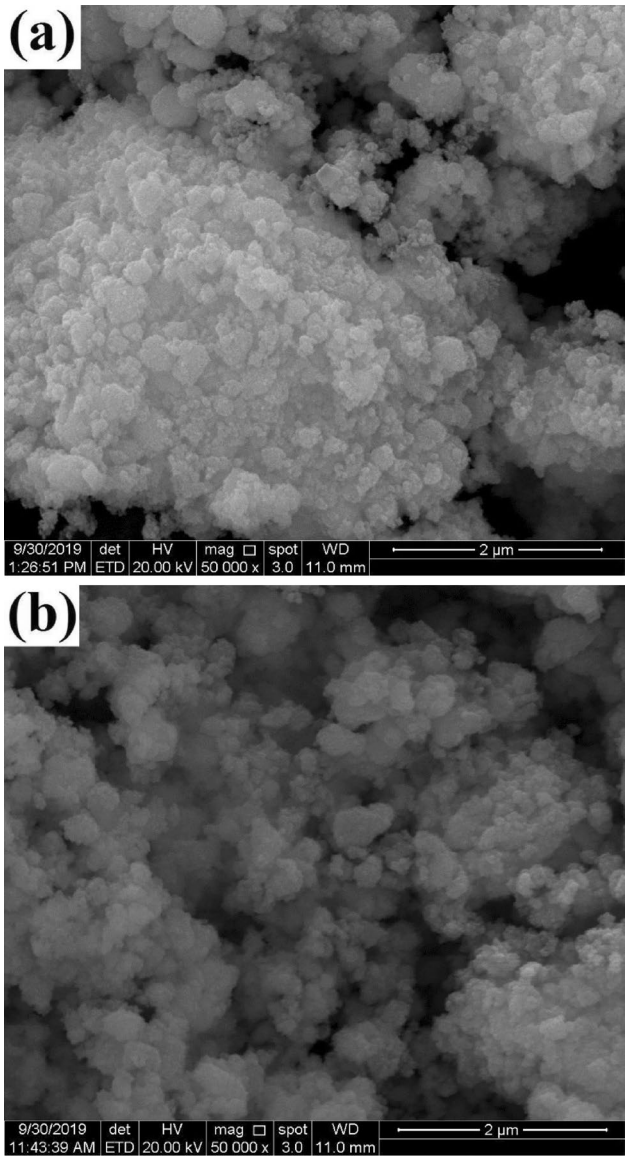

Fig. 2 FE-SEM images of **a**, **b** SnO_2 and **c**, **d** 7%SiC/SnO_2 composite

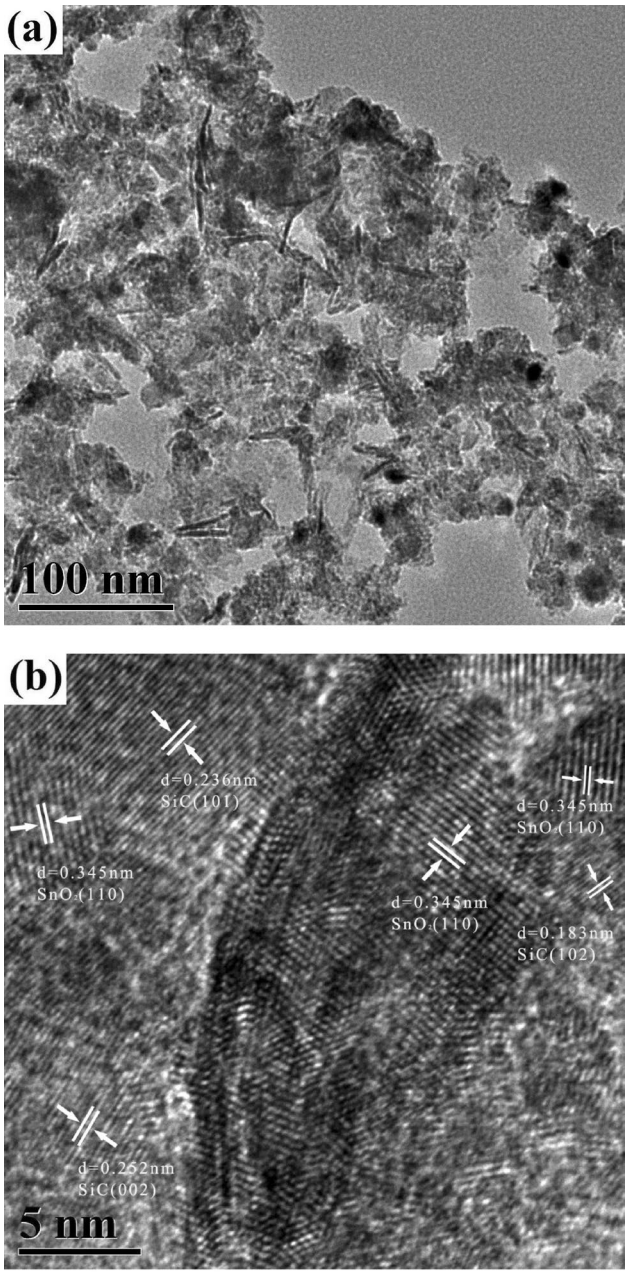

Fig. 3 The typical **a** TEM and **b** HRTEM images of 7%SiC/SnO_2 composite

Figure 4a shows the survey spectra, which confirmed the existence of Si, C, Sn, and O. As shown in Fig. 4b, the peaks centered at 486.98 and 495.38 eV are assigned to the $Sn3d_{5/2}$ and $Sn3d_{3/2}$ of Sn^{4+} in SnO_2, respectively. The O peaks (Fig. 4c) at 530.74, 531.81, and 534.29 eV are assigned to O–Sn–O, surface hydroxyl oxygen (–OH), and adsorption oxygen groups, respectively. Figure 4d and e show the high-resolution spectra of Si 2p and C 1s, respectively. The peaks centered at 101.8 and 284.6 eV are attributed to Si 2p and C 1s of SiC, respectively. The C=O bond mainly rose from oxygen absorbed on the surfaces of the SiC nanostructures.

The photoluminescence spectrum of the sample was recorded to investigate the separation effect of photogenerated electrons and holes in the composites (Fig. 5). The intensity of all emission peaks of SnO_2/SiC composites was

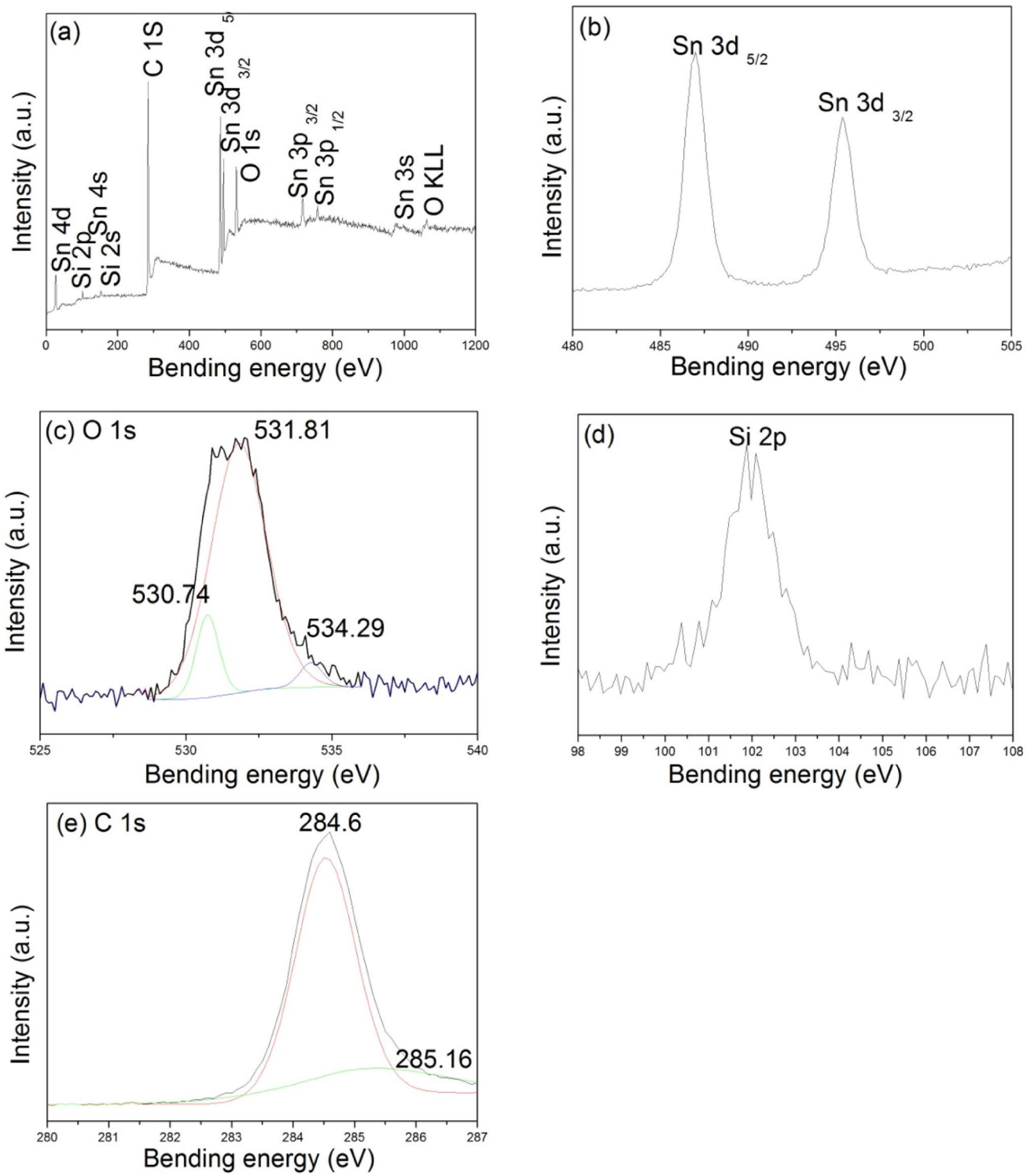

Fig. 4 The XPS spectra of **a** survey, **b** Sn 3d, **c** O 1s, **d** Si 2p and **e** C 1s for 7%SiC/SnO_2 composite

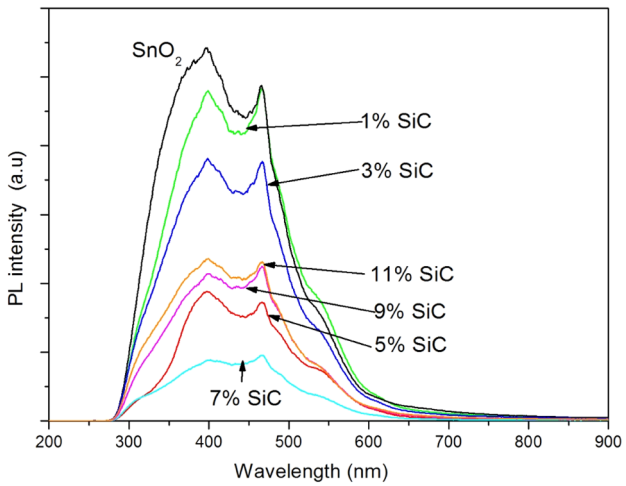

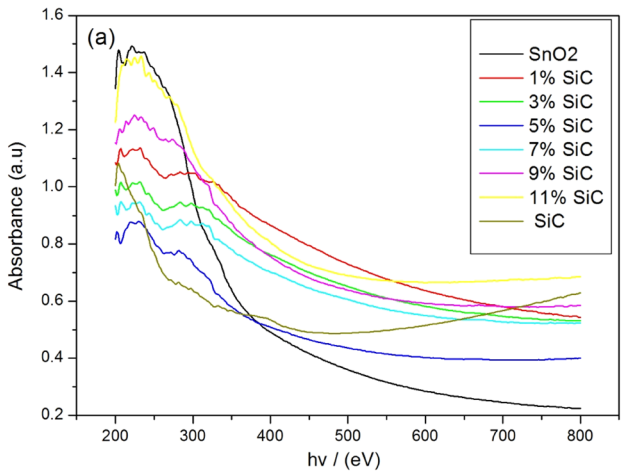

Fig. 5 Photoluminescence spectra of SiC/SnO_2 composites

lower than that of SnO_2, suggesting the low recombination probability of electron holes in the composites. The peak intensity of 7% SnO_2/SiC composite was the lowest, indicating that the electron–hole recombination probability of the catalyst was the lowest. This composite was considered the most conducive to the separation of electrons and holes in the photocatalytic system. Hence, the introduction of SiC effectively improved the luminescent properties of SnO_2 and rendered them conducive to photocatalytic reaction.

The typical UV–Vis diffuse reflection spectra of SiC, SnO_2, and composites are shown in Fig. 6a. SnO_2 showed weak absorption capacity, indicating that it possessed a wide band gap, whereas pure SiC had an obvious absorption band from 200 to 800 nm. SiC/SnO_2 composites had obviously stronger absorption capacity than SnO_2 in the visible region. These results indicated that the SiC/SnO_2 composites exhibited efficient visible-light utilization, which can result in good photocatalytic performance.

Figure 6b shows that the band-gap energy (E_g) values of SiC/SnO_2 composites were about 2.65 eV. Single-phase SnO_2 and SiC had a high E_g value of 2.78 and 2.99 eV, respectively. Thus, their combination significantly reduced their band gap, thereby improving the utilization efficiency of visible light.

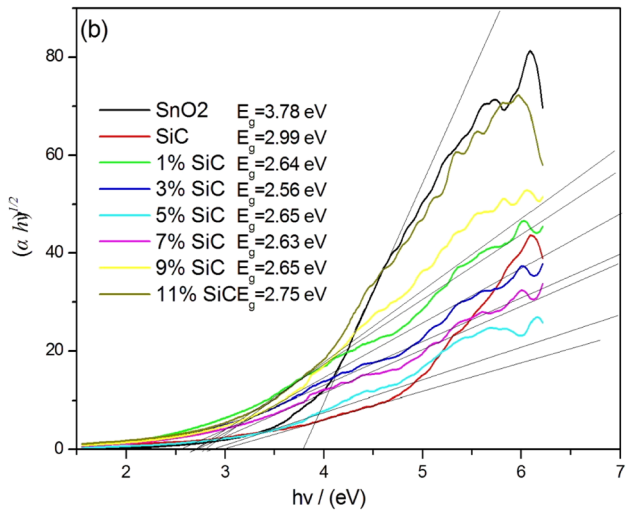

Fig. 6 **a** UV–Vis DRS spectra and **b** band gap energy (E_g) values of SiC/SnO_2 composites

Figure 7 compares the photocatalytic degradation of MO by SnO_2 and SnO_2/SiC composites under visible light. SnO_2 exhibited weak ability to photocatalytic degradation of MO. Moreover, SnO_2/SiC composites had good degradation ability. The photocatalytic degradation abilities of 1% SiC/SnO_2,

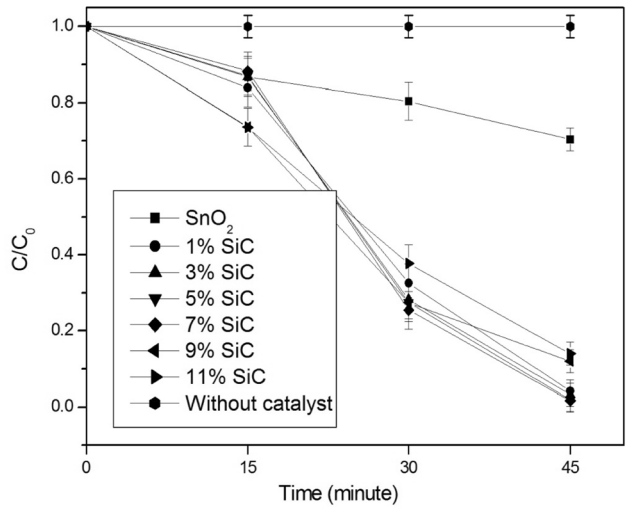

Fig. 7 The photocatalytic activity of the SiC/SnO_2 composites to MO dyes

3% SiC/SnO_2, 5% SiC/SnO_2, and 7% SiC/SnO_2 composites were better, and they degraded 99% MO within 45 min. The enhancement can be explained by the synergetic effect on the efficient electron–hole separation at the SnO_2/SiC photocatalyst interface. Figure 1 shows that the 9%SiC/SnO_2, and 11% SiC/SnO_2 composites contained some $Sn_6O_4(OH)_4$ impurity. Obviously, adding excess SiC inhibited the transformation of $Sn_6O_4(OH)_4$ to SnO_2, which decreased the content of SnO_2 photocatalysts in the composites.

Table 2 shows the visible photocatalysis results of the fabricated SnO_2/SiC composite and SnO_2-based catalysts in other studies. The SnO_2/SiC composite showed higher photocatalytic degradation rate than the other SnO_2-based photocatalysts. Hence, SnO_2/SiC photocatalyst could be a new highly efficient catalyst.

To evaluate the photocatatyic cyclic performance of the 7% SnO_2/SiC composite, four cycling experiments were performed for MO degradation. Figure 8a shows that after several cycles, no obvious change occurred in the photocatalytic-degradation activity. Additionally, the XRD (Fig. 8b) pattern and XPS (Fig. 8c–g) data remained stable. These findings indicated the reusability and high stability of the 7% SnO_2/SiC composite.

The proposed mechanism of photocatalytic degradation over SnO_2/SiC nanosheets is shown in Fig. 9. The locations of the conduction and valence bands of SiC and SnO_2 were confirmed by the Mott–Schottky plot. The valence-band maximum values of SiC and SnO_2 were estimated at 1.6 and 3.78 eV, and the corresponding conduction-band minimum values of SiC and SnO_2 were around − 1.4 and 0 eV, respectively. The conduction band of SiC was more negative than that of SnO_2, resulting in the transfer of electrons generated in the conduction band from SiC to SnO_2 nanoparticles. The valence band of SnO_2 was more positive than that of Si; as such, the hole transferred from the valence band of SnO_2 to the valence band of SiC. This migration of electrons and holes between SnO_2 and SiC effectively reduced the band gap of SnO_2. This phenomenon further improved the mobility of electrons, inhibited the recombination of electrons and holes,

Table 2 Photocatalytic activities of different SnO_2 matrix photocatalysts under visible light

Catalyst	Catalyst concentration (g L^{-1})	Dye concentration (mg L^{-1})	Time (min)	Degradation degree (%)	Ref.
SnO_2/SiC	1	MO(15)	45	99	Our work
SnO_2/TiO_2	0.5	MB (0.32)	360	29	6
SnO_2/ZnO	0.5	RhB(3.2)	360	49	7
Fe_2O_3/SnO_2	/	Acid blue 62 (50)	60	98	8
Fe_2O_3/SnO_2	1	MO(3.27)	180	73	9
SnO_2/graphene	0.1	MB(2.4)	60	83	10

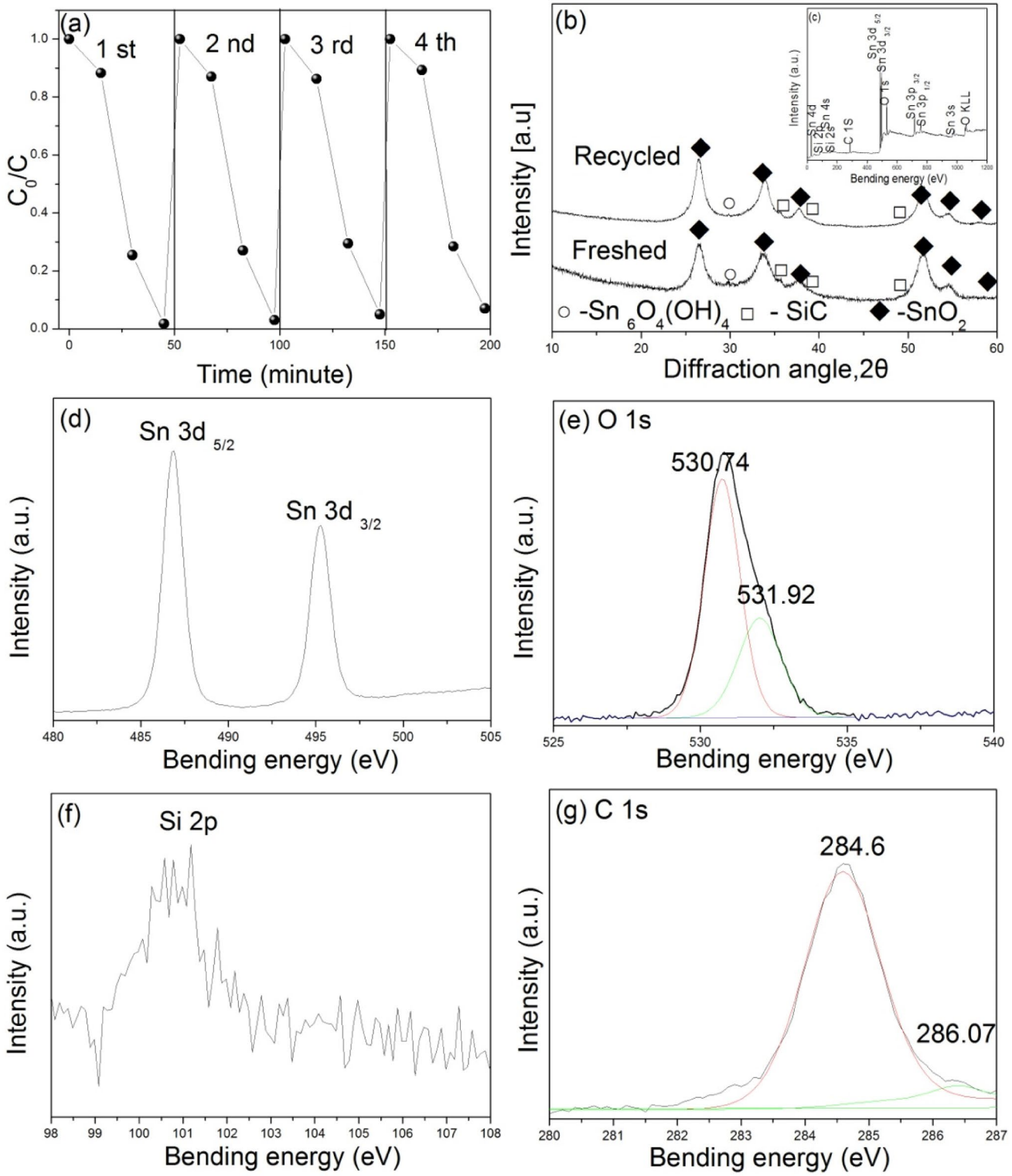

Fig. 8 The four recycled testing of 7% SnO_2/SiC composite for MO degradation (**a**), and the XRD pattern (**b**), XPS survey spectrum (**c**), high-resolution spectra of Sn 3d (**d**), O 1s (**e**), Si 2p (**f**) and C 1s (**g**) of the composite after cycles for MO degradation

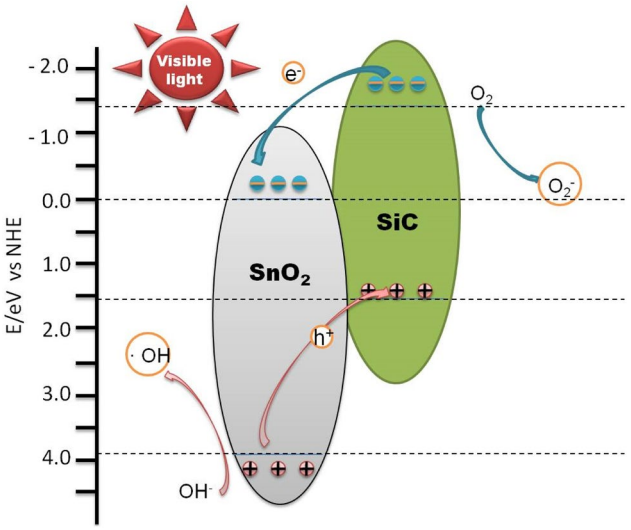

Fig. 9 The photocatalytic routes of the SiC/SnO_2 heterostructure

and prolonged the lifetime of electrons and holes, which are conducive to photocatalytic degradation. The holes in the valence band oxidized MO into CO_2 and H_2O and interacted with OH^- to form ·OH radicals, which also oxidized MO into CO_2 and H_2O. In addition, the electrons on the conduction band reduced the adsorbed O_2 into O_2^- and oxidized MO into CO_2 and H_2O.

4 Conclusions

In this work, SiC/SnO_2 composites were synthesized by mechanical alloying combined with aging. The TEM, XPS, UV–Vis DRS, and PL studies showed the formation of SiC/SnO_2 heterojunction, which inhibited the recombination of photogenerated electron–hole pairs. Hence, the fabricated SiC/SnO_2 composites exhibited excellent visible-light photodegradation of MO. In particular, 7%SiC/SnO_2 composite possessed the highest photodegradation rate, that is, it degraded 99% MO within 45 min.

Acknowledgements This project was sponsored by the National Natural Science Foundation of China (Grant No. 51864028), the Natural Science Foundation of Henan (18A430035), the Natural Science Foundation of Henan (Grant No. 18A430035), International S&T Cooperation Program of China (Grant No. 2015DFR50620).

References

1. A. Fujishima, K. Honda, Electrochemical photolysis of water at a semiconductor electrode. Nature **238**, 37–38 (1972)
2. R. Raliya, C. Avery et al., Photocatalytic degradation of methyl orange dye by pristine titanium dioxide, zinc oxide, and graphene oxide nanostructures and their composites under visible light irradiation. Appl Nanosci **7**, 253–259 (2017)
3. M. Ritu, K. Vijay, J. Nirav et al., Au–TiO_2-loaded Cubic g-C_3N_4 nanohybrids for photocatalytic and volatile organic amine sensing applications. ACS Appl Mater Int **10**, 34087–34097 (2018)
4. P.A. Aprilya, W. Sri, P.P. Yuniar et al., Optimisation of methyl orange photodegradation using TiO_2-zeolite photocatalyst and H2O2 in acid condition. IOP Conf Ser: Mater Sci Eng **546**, 042047–042055 (2019)
5. N. R.Zha, X.Guo Reddeppa et al., Ultraviolet photocatalytic degradation of methyl orange by nanostructured TiO_2/ZnO heterojunctions. J Mater Chem A **3**, 6565–6574 (2015)
6. D. Venkatesh, S. Pavalamalar, K. Anbalagan, Selective photodegradation on dual dye system by recoverable nano SnO2 photocatalyst. J Inorg Organomet Polym **29**, 939–953 (2019)
7. M.U. Khalid, S.R. Khan, S. Jamil, Morphologically controlled synthesis of cubes like tin oxide nanoparticles and study of its application as photocatalyst for congo red degradation and as fuel additive. J Inorg Organomet Polym **28**, 168–176 (2018)
8. L. Mohan, N. Sisupalan, K. Ponnusamy et al., One step synthesis and characterization of ZnO–ZnSe heterostructures by chemical precipitation and its solar photocatalytic activity. J Inorg Organomet Polym **30**, 2626–2632 (2020)
9. A. Phuruangrat, P. Keereesaensuk, K. Karthik et al., Synthesis and characterization Ag nanoparticles supported on Bi_2WO_6 nanoplates for enhanced visible-light-driven photocatalytic degradation of rhodamine B. J Inorg Organomet Polym **30**, 1033–1040 (2020)
10. S. Weerachai, The self-cleaning and photocatalytic properties of TiO_2 doped with SnO_2 thin films preparation by sol-gel method. Energy Proc **89**, 170–176 (2016)
11. P. Petronela, A. Anton, O. Niculae et al., Photocatalytic degradation of rhodamine B dye using ZnO–SnO_2 electrospun ceramic nanofibers. Ceram Int **42**, 6775–6781 (2016)
12. H.L. Xia, H.S. Zhuang, T. Zhang et al., Visible-light-activated nanocomposite photocatalyst of Fe_2O_3/SnO_2. Mater Lett **62**, 1126–1128 (2008)
13. Y.P. Zang, L.P. Li, X.G. Li et al., Synergistic collaboration of g-C_3N_4/SnO_2 composites for enhanced visible-light photocatalytic activity. Chem Eng J **246**, 277–286 (2014)
14. B. Quan, W. Liu, Y.S. Liu et al., Quasi-noble-metal graphene quantum dots deposited stannic oxide with oxygen vacancies: synthesis and enhanced photocatalytic properties. J Colloid Interf Sci **481**, 13–19 (2016)
15. J. Weng, P. Lee, Y. Chen et al., Degradation of abiotic orange II dye and biotic *E. coli* by highly porous SiC-AgCl/Ag0 photocatalyst. J Inorg Organomet Polym **30**, 1760–1768 (2020)
16. J.Y. Hao, Y.Y. Wang, X.L. Tong et al., Photocatalytic hydrogen production over modified SiC nanowires under visible light irradiation. Int J Hydrog Energy **37**, 15038–15044 (2012)
17. C.Y. Li, H.B. Ouyang, J.F. Huang et al., Synthesis and visible-light photocatalytic activity of SiC/SiO_2 nanochain heterojunctions. Mater Lett **122**, 125–128 (2014)
18. J.J. X.Liao, M.M. Chen, Wang et al., Enhanced photocatalytic and photoelectrochemical activities of SnO_2/SiC nanowire heterostructure photocatalysts. J. Alloys Compd **658**, 642–648 (2016)
19. X.L. Zhang, D. Shao, W. Lyu et al., Utilizing discarded SiC heating rod to fabricate SiC/Sb-SnO_2 anode for electrochemical oxidation of wastewater. Chem Eng J **361**, 862–873 (2019)
20. B.Y. Liang, Mechanical-induced spontaneous formation of SnO_2/$Sn_6O_4(OH)_4$ photocatalysts at room temperature. Mater Lett **252**, 155–157 (2019)